Proceedings World Geothermal Congress 2015
Melbourne, Australia, 19-25 April 2015

Decision Making Software for Forecasting Induced Seismicity and Thermal Energy Revenues in Enhanced Geothermal Systems

Dimitrios C. Karvounis and Stefan Wiemer

Swiss Seismological Service (SED), ETH Zurich, NO H 62, Sonneggstrasse 5, 8092 Zurich, Switzerland

karvounis@sed.ethz.ch and stefan.wiemer@sed.ethz.ch

Keywords: EGS, induced seismicity, modeling, hazard assessment

ABSTRACT

The development of many novel deep geothermal technologies, such as Enhanced Geothermal Systems (EGS), has decelerated due to induced seismicity. Sophisticated traffic light systems, which assess the efficiency of the implemented stimulation strategy in time for altering it, can assist in successfully developing the EGS technology. Here is presented the modeling approach for a hybrid model that combines numerical calculations with stochastic geo-mechanical modeling and which can be used from such a traffic light. This hybrid model can assist in probabilistically assessing both the induced seismicity hazard and the thermal energy revenues that should be expected from the decided stimulation strategy. The numerical part is performed by HFR-Sim. HFR-Sim is an EGS simulator that numerically solves flow and heat transport problems inside 3D dynamically changing fracture networks. It offers discrete fracture representation and it can simulate a wide range of scenarios that are EGS related. The stochastic computations are performed by a 3D seed model, which has been used by the Swiss Seismological Service (SED) for forecasting induced seismicity hazard. It stochastically samples possible earthquakes (so called seeds) and by considering simple failure criteria, it decides which seeds are triggered and when. Here, the main elements of this hybrid model and the coupling between them are discussed. The model is tested on a realistic exemplary scenario and its behavior is discussed.

1. INTRODUCTION

The increase of greenhouse gases in the atmosphere and the resulting concern for undesired climate change has led many industrialized countries to the establishment of an international regulatory framework for the reduction of CO_2 emissions. Fossil-fuel power plants are associated with high international costs and 'environment friendly' base load energy production technologies are favored. Geothermal power plants have low greenhouse emissions, can uninterruptedly supply thermal and electrical power and thus, they can cover a portion of the base load energy needs. According to estimations, the electrical power production with geothermal technology is expected to rise to *70 GWe* by the year 2050, where additional *70 GWe* of electrical power could be produced if Enhanced Geothermal Systems (EGS) or other deep geothermal technologies are successfully developed (Bertani, 2012).

EGS (or Petrothermal) technology extracts heat from reservoirs that are located at drillable depths and does not require significant quantities of water to be already in place. Once the EGS wells are drilled and before any power is produced, the wells need to be stimulated. Cold fluid (usually water) is injected at high pressure through each well to induce hydro-shearing and hydro-fracking, aiming to artificially enhance the permeability of the EGS reservoir. Thermal energy cannot be produced efficiently unless the impedance between the EGS wells is reduced and large flow rates can be circulated inside the EGS reservoir. Such reservoir stimulations are considered successful when the resulting impedance allows the circulation of fluids at commercially interesting flow rates, while the induced seismicity causes neither nuisance nor damage.

The development of EGS technology has decelerated due to the induced seismicity hazard. A *3.4* magnitude earthquake was induced in an EGS project in Basel, Switzerland, during the stimulation of its reservoir (Kraft et al. 2009) and resulted to the cancelation of the project there. Urban environments are areas of prime location for the development of geothermal power plants. The waste heat, which cannot be converted to electricity, can be directly utilized for heating purposes there. However, as it was the case in Basel, the EGS technology cannot be applied in such locations unless the induced seismicity hazard is kept low.

Traffic light systems can assist in assessing the induced seismicity hazard in real time and can assist in critical decision making that needs to take place during the stimulation of an EGS reservoir. Such a new sophisticated traffic light system is currently under development by the Swiss Seismological Service (SED) and will be used for real time Probabilistic Induced Seismicity Hazard Assessment (PISHA). During stimulation, all the field data (both real time observations and prior information) are collected, pre-processed and used by a variety of models that forecast induced seismicity and allow the hazard and risk assessment. Figure 1 illustrates the framework for this traffic light system. It is important that all PISHA calculations are performed in real time; i.e. the traffic light needs to return the results to the reservoir operators in time for altering the implemented stimulation strategy. This need for fast calculations prohibits the use of computationally expensive models. The uncertainty regarding the reservoir properties during stimulation favors the use of less expensive models, since these models can forecast induced seismicity for a large number of different scenarios and thus, they can partially treat uncertainty.

Hence, statistical and hybrid models are usually used. Bachmann et al. (2011), and Mena et al. (2013) have tested different statistical methods that were partly able to forecast expected seismicity for six hours in advance and are based on the applied injection rates. Some of the statistical models that were tested are approaches similar to the Epidemic Type Aftershock Model (Ogata, 1992) and to the seismogenic index for each site (Shapiro et al., 2010). Statistical methods return results very quickly, but they are solely data-based and can forecast the injection-induced seismicity for a short period of time. Hybrid models, which couple pressure solutions with stochastic geo-mechanical modeling (the so-called 'seed model'), can forecast seismicity for longer periods

of time. The seeds are potential earthquake locations which are distributed in space and can be triggered only by elevated fluid pressure. Goertz-Allmann and Wiemer (2013) used the analytical solution of the linear pressure diffusion problem of a source point inside a homogeneous and isotropic reservoir in order to trigger the seeds, while Gischig and Wiemer (2013) used the COMSOL software, with which they numerically solve a line source non-linear and one-dimensional pressure diffusion problem. Both hybrid models were calibrated with the wellhead pressure curve and the seismicity characteristics of the Basel stimulation experiment in 2006 and demonstrated forecasting capabilities.

However, these hybrid models consider reservoirs of reduced dimensions, where permeability is always isotropic and thus the pressure fronts of highly fractured three-dimensional EGS reservoirs cannot be captured representatively. Fine spatial pressure variations rarely show up, important information, such as the position and the orientation of large fractures, is neglected and the injection strategy is never tested towards the commercial target for financial sustainability, since heat transport modeling is not included.

Contrary to continuum methods, Discrete Fracture Models (DFMs) use fewer simplifications in modeling fractures and can treat the above issues. DFMs have been employed by many EGS simulators since they are considered an important feature for EGS simulations (Sanyal, 2000), but have not been used for real tine PISHA, since they usually require prescribing of all foreseeable fractures. The FRACAS code (Bruel et al., 2001) employs a DFM where all fractures are disc-shaped and are embedded in an impermeable medium. Thus, the pressure front can only reach prescribed fractures. Kohl et al. (1995) apply the Finite Element Method and perform hydraulic, mechanical and heat transport modeling on a grid for which it is mandatory that the rock elements conform to the shape of the discrete fractures. A similar approach with a conforming grid is adopted by McClure and Horne (2011), where the Displacement Discontinuity (DD) method is coupled with a flow simulator that also requires a conforming grid. Both approaches, cannot easily adapt to not foreseeable changes of the fracture network, since re-meshing and re-calculating all the properties on the new mesh is required.

Embedded DFMs avoid this computational cost and can be adaptive to dynamically changing fracture networks. They treat discrete fractures as lower dimensional source/sink manifolds embedded in a permeable medium. They combine advantages both from CFM and DFM approaches. New discrete fractures can be included without the need of re-meshing and computationally expensive and complex grids are avoided. The EGS simulator HFR-Sim (Karvounis and Jenny 2011, Karvounis 2013) employs such an embedded DFM for the modeling of flow and heat transport in an EGS reservoir.

Here, the modeling framework for a three-dimensional hybrid model that employs DFM is presented. It aims to combine the seed model approach with more realistic solutions for the pressure field inside an EGS reservoir. Modeling of flow and heat transport is treated by a modified version of HFR-Sim, while the seed model by Gischig and Wiemer (2013) is extended into three dimensions. Triggered seeds are modeled by HFR-Sim as fractures that suddenly become significantly more permeable and thus, are treated as discrete fractures thereafter. The triggered seeds create a network of fractures which is modeled by HFR-Sim. The expected revenues of thermal power for each such fracture network can be estimated by HFR-Sim afterwards. This new hybrid model will be used in the future for real time PISHA and simultaneously will assess the expected thermal revenues.

2. THREE-DIMENSIONAL HYBRID DISCRETE FRACTURE MODEL

During the PISHA calculations, each hybrid model needs to be used numerous times until a large number of equally probable synthetic catalogs are produced. This allows estimating the probability of inducing a seismic event that has a magnitude larger than a certain value. Additionally, simulations of the production phase need to be performed for a subset of those scenarios. This will allow estimating the expected thermal revenues for a given stimulation strategy.

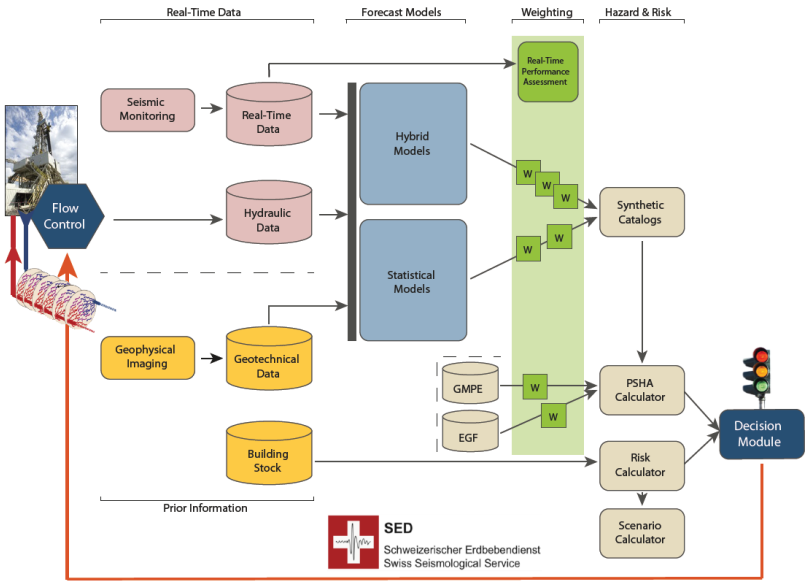

Figure 1: The algorithmic framework for the real time traffic light system is illustrated above. The hybrid and the statistical models, post-process the real time data and prior information, in order to return synthetic catalogs. These catalogs are used for performing PISHA and for changing the injection rate accordingly. The image is adapted by the webpage of the Induced Seismicity group in SED.

The hybrid model that is presented here consists of the HFR-Sim software and the stochastic 'seed model'. At the beginning of each simulation, an HFR-Sim model is constructed, which consists of the well, some discrete fractures and an effective continuum. The time-marching simulation starts afterwards. At each time step, HFR-Sim returns an approximation of the pressure distribution and subsequently, the seed model performs all the geomechanical modeling; i.e. it decides which seeds have high enough pressure to be triggered. Before proceeding to the next time step the network of discrete fractures is updated. Creation phase can be simulated for numerous days after injection has been stopped. Once the creation phase is simulated, then HFR-Sim can simulate scenarios of the production phase for the resulting network of fractures. It is noted, that the HFR-Sim model that is constructed at the beginning of the simulation is expected to include many of the field observations. However, history matching approaches for this kind of problems are not discussed here.

2.1 Flow and heat transport calculations with HFR-Sim

Henceforth, a three-dimensional EGS reservoir domain $\Omega \in \boldsymbol{R}^3$ is considered. Single phase Darcy flow takes place everywhere inside it. The Oberbeck-Boussinesq approximation is assumed, according to which variations of fluid density ρ can be neglected, if they are not multiplied with the gravitational acceleration $|\boldsymbol{g}|$, where $\boldsymbol{g}$ is the vector for gravitational acceleration.

Mass conservation on Ω and in a Cartesian grid can now be expressed as

$$\frac{\partial \varphi}{\partial t} - \nabla \cdot \left(\frac{\boldsymbol{k}}{\mu} \cdot \left(\nabla p - \rho \boldsymbol{g} \nabla z \right) \right) = q, \tag{1}$$

where q is a source term, φ the porosity, μ the dynamic fluid viscosity, $\boldsymbol{k}$ the permeability tensor, p the fluid pressure and z the depth. According to Darcy law, the fluid velocity $\boldsymbol{u}$ inside Ω equals $\boldsymbol{u} = \frac{\boldsymbol{k}}{\mu} \cdot \left(\nabla p - \rho \boldsymbol{g} \nabla z \right)$. Here, the density ρ and the viscosity μ of the fluid are assumed constant.

Energy conservation inside domain Ω can be expressed as

$$\frac{\partial h}{\partial t} - \nabla \cdot \left(\boldsymbol{\lambda} \cdot \nabla T \right) + \nabla \cdot \left(\boldsymbol{u} h \right) = w, \tag{2}$$

where h denotes the specific enthalpy, tensor $\boldsymbol{\lambda}$ the heat conductivity of the material, T the temperature and w is a heat source term.

Here, both the flow and the heat transport modeling are treated by HFR-Sim, which employs an adaptive hierarchical embedded DFM. Large dominant fractures are treated as lower dimensional manifolds and are embedded inside a continuum that is called 'damaged matrix' and captures the effect of the small fractures. The damaged matrix is divided into smaller control volumes by a rather coarse and structured grid. Each large fracture is also discretized by a lower dimensional structured grid, where the boundaries of the cells of large fractures do not have to conform neither to the boundaries of the cells for the damaged matrix nor to the boundaries of the cells that belong to other large fractures. Figs. 2a-2c illustrate such a gridding.

The resulting HFR-Sim mesh is unstructured and consists of many independent structured grids. Hence, HFR-Sim avoids tiny fracture volumes that would reduce the time-step size and increase the computational cost. New discrete fractures can be added to the computational domain of HFR-Sim without the need of re-meshing and re-computing the fluid properties on a new mesh. A new discrete fracture is added simply by adding few more control volumes and their connections to the existing grid.

For each pair of control volumes M, J the transmissibility $C_{M,J}$ is calculated, such that volume flux from volume M to volume J equals $F_{M,J} = C_{M,J} (P_M - P_J - \left(Z_M - Z_J \right) \rho | \boldsymbol{g} |)$, with Z_M corresponding to the average depth of volume M and P_M is the mean fluid pressure inside control volume M. Transmissibility $C_{M,J}$ is non-zero only when volumes M and J are permeable and either they intersect each other or their boundaries are adjacent. The transmissibility $C_{M,J}$ is computed for each cell according to Karvounis (2013) and depends on the permeability of the two cells as well as the size of the area through which flow occurs and the average distance between the two volumes. Fig. 2d shows connections between the fracture cells of this gridding example, which have a non-zero transmissibility $C_{M,J}$.

HFR-Sim also employs a simple well model. The fluid pressure along the open case of the well is considered constant and thus, each open case well corresponds to a single control volume. Connections are also introduced between the control volume of a well and intersecting cells. When either the cell M or the cell J is a well volume, then $C_{M,J}$ is equal to the production index of the well. This production index is similar to the well model suggested by Peaceman (1978).

The equation of mass conservation (1) results into a discretized system of N equations, where N is the total number of nodes in the unstructured HFR-Sim grid and each equation M is

$$\frac{\partial V_M}{\partial t} + \sum_{J=1}^{N} C_{M,J} (P_M - P_J - \left(Z_M - Z_J \right) \rho | \boldsymbol{g} |) = Q_M \,, \tag{3}$$

where Q_M is the rate of the injected fluid and V_M is the size of the volume M.

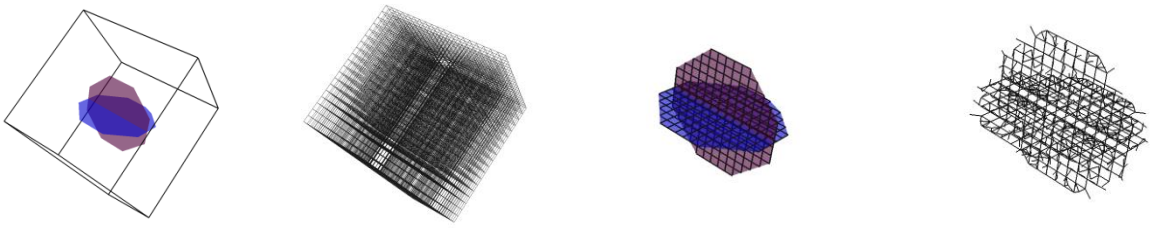

(a) EGS reservoir model

(b) HFR-Sim nodes and connection (lines) for the damaged matrix

(c) HFR-Sim nodes and connections for each discrete fractures

(d) Discrete fracture nodes and their connections to matrix or different fracture cells.

Figure 2: (a) Illustration of the hydraulic coupling between two large 2D fractures and a 3D damaged matrix. (b) A simple structured grid is employed for the damaged matrix. (c) Each large fracture is discretized by a simple 2D orthogonal structured grid and only nodes within the permeable area of the fracture are considered by HFR-Sim. (d) Further connections are added that couple each cell from a large fracture with the damaged matrix cells, as well as cells from other large fracture, that intersect it.

Henceforth, it is assumed that $\frac{\partial V_M}{\partial t} = 0$, if *M* is a well volume, and $\frac{\partial V_M}{\partial t} = \frac{\partial V_M}{\partial P_M}\frac{\partial P_M}{\partial t}$, otherwise. The derivative $\frac{\partial V_M}{\partial P_M}$ is treated as constant and does not change neither with pressure nor with time.

The solid rock domain can be decomposed with a structured grid into N^r control volumes, where each control volume *m* has a size $\left|\Omega_m^r\right|$ and equation (2) can be explicitly discretized with a system of N equations. Energy conservation for each node *M* becomes

$$\frac{\partial \hat{H}_M}{\partial t} + \sum_{J=1}^{N} F_{M,J}\left(H\left(F_{M,J}\right)\hat{H}_M + H\left(-F_{M,J}\right)\hat{H}_J\right) = W_M + \sum_{m=1}^{N^r} K_{m,M}^r\left(T_m^r - T_M\right), \tag{4}$$

where $\hat{H}_M$ is the amount of enthalpy stored in volume *M*, $H(\cdot)$ is the Heaviside step function that is introduced here instead of the upwind scheme that is employed, $K_{m,M}^r$ are the effective coefficients that quantify energy fluxes from the hot rock to the working fluid, T_M the mean temperature inside volume *M* and T_m^r the mean temperature inside rock volume *m*.

Energy conservation for each solid rock *m* gives

$$\frac{\partial \hat{H}_m^r \left|\Omega_m^r\right|}{\partial t} + \sum_{j=1}^{N^r} K_{m,j}^r\left(T_m^r - T_j^r\right) = W_m^r\left|\Omega_m^r\right| + \sum_{M=1}^{N} K_{m,M}^r\left(T_M - T_m^r\right), \tag{5}$$

where $\hat{H}_m^r$ is the amount of enthalpy stored in rock volume, $K_{m,j}^r$ quantifies head diffusion from rock volume *m* to and W_m^r is the mean value of source term *w* inside volume *m*.

Finally, it is noted that HFR-Sim uses an algebraic multigrid (AMG) solver with a Gauss-Seidel method as a smoother. The solver is used in order to solve equation (3) implicitly

2.2 Seed model

We consider a number of N_s potential earthquake locations (seeds) which are uniformly distributed in space. Each seed *i* is located at $\boldsymbol{x}^i=(x^i, y^i, z^i)^T$ and lays on a fault with pole unit vector $\boldsymbol{P}^i$. Three principal compressive stress vectors $\boldsymbol{\sigma}_1^i, \boldsymbol{\sigma}_2^i \text{ and } \boldsymbol{\sigma}_3^i$ that are representative of the ambient stress field as well as friction coefficient μ_c^i and cohesion C^i are assigned to each seed *i*. The normal stress vector $\boldsymbol{\sigma}_n^i$ and shear stress vector $\boldsymbol{\tau}_n^i$ can be computed analytically for each seed point. The value of the effective normal stress equals to

$$\sigma_{n,eff}^i = \left|\boldsymbol{\sigma}_n^i\right| - P_{hydro} - p\left(\boldsymbol{x}^i\right), \tag{5}$$

where P_{hydro} is the hydrostatic pressure. Here, the pressure of the fluid *p* is interpolated from the results returned by HFR-Sim and is the only term in equation (5) that changes with time.

A fault slips around the seed point *i* and an earthquake is triggered, when the Mohr-Coulomb failure criterion is satisfied and

$$\left(\left|\tau_n^i\right| - C^i\right)/\sigma_{n,eff}^i > \mu_c^i. \tag{6}$$

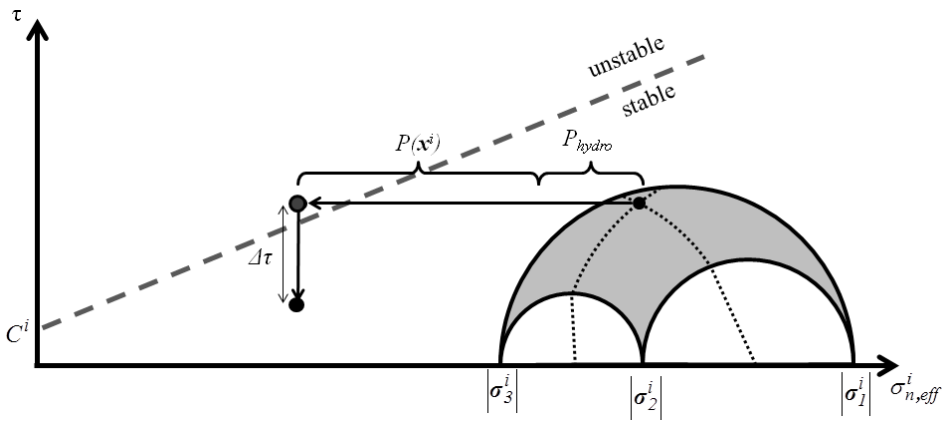

Figure 3: Three principal compressive stresses are assigned to each seed *i* as well as an orientation (pole vector). Thus, effective normal and shear stress can be computed on the seed. The seed approaches the unstable region with increasing fluid pressure *p*. When the seed crosses the Mohr-Coulomb failure line then the seed triggers and an earthquake event with stress drop $\Delta\tau = 3.0$ *MPa* is considered.

A b^i value, which describes a Gutenberg-Richter distribution, is assigned to each seed point when it is triggered. This b^i value increases linearly as the differential stress $\Delta\sigma^i = \left(|\sigma_1^i| - |\sigma_3^i|\right)$ decreases. Afterwards, a random magnitude M_w^i is drawn from a Gutenberg-Richter distribution with the b-value b^i.

The fault is here assumed to have the shape of a circle which is centered in $\boldsymbol{x}^i$ and the vector $\boldsymbol{P}^i$ is normal to it. Moment M_o^i is computed from M_w^i by using the Hanks and Kanamori (1979) relationship

$$M_0^i = 10^{1.5(M_w^i + 6.03)} . \tag{7}$$

The stress drop $\Delta\tau^i$ is considered constant for all earthquakes and equal to $\Delta\tau = 3.0$ *MPa*. According to Eshelby (1957), the radius size r^i of such a slip is

$$r^i = \sqrt[3]{\frac{6M_0^i}{17\Delta\tau}} . \tag{8}$$

When the radius size r^i of an earthquake justifies discrete fracture representation, then a 'new' discrete fracture that represents the slipped fault segment is introduced in the HFR-Sim flow model.

2.3 Update of flow model

An EGS reservoir is a highly fractured hot rock and thus, domain Ω is characterized by a highly heterogeneous and anisotropic permeability tensor $\boldsymbol{k}$. Along the fractures the permeability tensor can be many orders of magnitude larger than the permeability across them or the permeability on the intact hot rock, while the permeability tensor $\boldsymbol{k}$ can even be considered discontinuous across the two surface planes of a fracture. Moreover, the permeability tensor can also change dynamically, e.g. when the permeability of fractures increases due to hydro-shearing or new fractures are created due to hydro-fracking. Thus, the accurate solution of Eqs. (1) and (2) without a discrete representation of fractures can be very challenging problem.

Initially, it is assumed that the domain Ω is a single porosity continuum with an isotropic and homogeneous permeability $\boldsymbol{k} = \boldsymbol{k_0}$. All wells are inside this continuum. The continuum consists of a single huge cluster of fractures, which is above the percolation threshold and penetrates both the drilled wells and the far-field boundaries. Thus, the injected fluid can reach and can induce earthquakes anywhere inside Ω. The value of this effective intact permeability $\boldsymbol{k_0}$ and of the specific storage of the reservoir can be estimated with an injection test to the pre-stimulated reservoir (e.g. by injecting at very low rates for a long period of time). Therefore, they are treated as known values here.

When fault *i* slips, then its permeability increases. This permeability increase depends on the resulting hydraulic aperture b_h^i of the slipped fault, i.e. the permeability on the fault equals $\boldsymbol{k} = (b_h^i)^3/12$. This permeability change and the newly created void volume $V^i = \pi (r^i)^2 b_h^i$ affect the flow in the reservoir and this effect needs to be taken into account.

When the radius of the slipped area is larger than half the grid-block length, then a discrete fracture is added to the HFR-Sim model and nothing else needs to change in the pre-existing mesh.

Otherwise, when the radius of the slipped area is smaller than $(\Delta x/2)$, then the permeability of the damaged matrix cell, inside which the earthquake occurred, may need to be increased. For such small earthquakes there is a lot of uncertainty both for their exact position in space and for their connectivity with other slipped faults. The existence of a small earthquake inside a grid-cell does not necessarily increase the effective permeability of this cell (Figs. 4a-4b). Also, permeability does not always increase

seismically. For example, the permeability of a small fault may also increase due to the shearing of other faults and wing-cracks may be created that improve connectivity (McClure 2012, Jung 2013).

Here, the permeability inside the damaged matrix cell *M* increases only when the fracture density $\rho_3^{'}$ inside volume *M* is above a critical value

$$\rho_3^{'} = \frac{\pi^2 \sum \left(r_M^j\right)^3}{V_M} > \rho_{3c}^{'}, \tag{9}$$

where the slipped area r_M^j corresponds to a triggered seed *j* that is located inside volume *M*. This non-dimensional fracture density characterizes the connectivity of three-dimensional networks of disk-shaped fractures (Mourzenko et al., 2005).

At the end of each time-step, all the earthquakes that have occurred inside the cube-shaped cell *M* since the beginning of the simulation, are located and sorted such that $r_M^j > r_M^k$ for $j<k$. The effective permeability of the cell *M* is now computed as

$$k_M = k_0 + \frac{1}{\Delta x}\left(\frac{\left(b_h^{n_1^M}\right)^3}{12 \cdot \sum_1^{n_1^M} r^j} + \frac{\left(b_h^{n_2^M}\right)^3}{12 \cdot \sum_{n_1^M+1}^{n_2^M} r^j} + \cdots \right), \tag{10}$$

where n_i^M is the smallest integer for which the slipped areas r_M^j satisfy the condition of eq. (9) with $n_{i-1}^M < j \leq n_i^M$ and it is assumed that b_h^i does not decrease with increasing r_M^j.

In general, effectivizing small fractures reduces the accuracy of the employed hierarchical DFM. However, equation (10) still captures many features which are required in order to simulate in real time such an unconventional reservoir. Permeability k_M increases only when the criterion (9) is satisfied. This can be a grid independent criterion and favors permeability increase along large slipped areas. Earthquakes that have a small ruptured area influence a domain around them which is much smaller than the uncertainty of their location. Therefore treating them deterministically is not important and a probabilistic approach (percolation theory) is favored instead (Figs. 4a-b). This probabilistic approach takes into account the unavoidable uncertainty regarding the underlying fracture network and permeability does not necessary increase when a tiny earthquake occurs. Last but not least, the number of parameters that need to be calibrated remains small and the flow model can be calibrated quickly with the observed seismicity.

When the volume *M* is not penetrated by a large discrete fracture, then the critical fracture density is $\rho_{3c}^{'} = 3.6$, and it is $\rho_{3c}^{'} = 1.8$, otherwise (Figs. 4C-4d). These two values are very close to the percolation threshold of three-dimensional circle-shaped fracture networks with power-law size distribution (Mourzenko et al., 2005). As explained there, when this critical value is exceeded then it is more than 50% probable that there exists one fracture network which is above the percolation threshold. . In our case, the fracture density is estimated only by the shear slipped areas and thus it is safe to assume that there is much more than 50% probability that such a fracture network exists when the fracture density is larger than this critical value. Then, it is assumed that this fracture network is above the percolation threshold and it is significantly more permeable than $\boldsymbol{k_0}$.

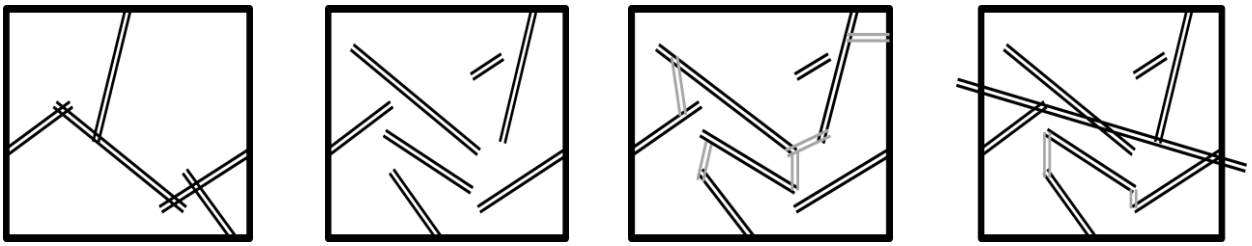

(a) percolated squared grid-block

(b) non-percolated squared grid-block

(c) grid-block without large fractures: $\rho_{3c}^{'} = 3.6$

(d) grid-block with large fractures: $\rho_{3c}^{'} = 1.8$

Figure 4: Simplified 2D scenarios of small fractures inside a squared grid-block. In (a) these fractures create a network which significantly increases the effective permeability. In (b) the previous fractures are repositioned and more fractures are considered, but the increase of the effective permeability is significantly less. In (c) and (d) fractures that become more permeable both due to shearing (black) or other failure mechanisms (grey) are considered and the assumed critical fracture density for each scenario is given.

3. EXEMPLARY SIMULATION

Here, an exemplary simulation with the hybrid model is presented. Initially, the stimulation of an EGS well is simulated and then a production phase simulation is performed for this stimulated reservoir.

The HFR-Sim model of the EGS reservoir has the shape of a cube, where each of its sides is *1.6 km* and the bottom of the reservoir lies at a depth of *5.76 km*. The open case of the well is *368.0 m* long, has a radius of *0.18 m*, reaches a depth of *5.0 km* and is centered inside the cube-shaped EGS reservoir. Initially, the model has no discrete fractures inside it and only the damaged matrix continuum is considered.

The permeability of the damaged matrix is $5 \cdot 10^{-17}\ m^2$ and its porosity $\varphi = 1\%$. The injected working fluid has constant density $\rho = 10^3\ kg/m^3$ and constant viscosity $\mu = 2.5 \cdot 10^{-3}\ Pa \cdot s$, while gravitational effects are not considered here. It is also assumed that $\left(\partial\varphi / \partial p\right) = 10^{-11}\ Pa^{-1}$ for the damaged matrix and the term $\left(\partial V_M / \partial P_M\right)$ can be derived accordingly. All specific heat capacities and densities are treated as constants. The specific heat capacity of the working fluid is $c_p = 4.18 \cdot 10^3\ J/kg/^oC$, the density of the hot rock is $\rho^r = 2.7 \cdot 10^3\ kg/m^3$ and its specific heat capacity $c_p^r = 920\ J/kg/^oC$. Also, the temperature profile of the hot rock is similar to the one measured in Basel. It is noted that this initial HFR-Sim model has many similarities with models of the pre-stimulated EGS reservoir in Basel.

3.1 Stimulation of EGS well

At time *t=0 s* fluid injection begins and the reservoir is stimulated with a four step injection scenario, where the injection rate increases by *10.0 l/s* every day. Fluid is injected during the first 4 days, the well shuts down afterwards and the simulation ends after 30 days. Fig. 5a shows the injection scenario for the simulated period. All slipped faults have the same aperture value $b_h^i = b = 10^{-4}\ m$ and therefore the fracture permeability is always $|\boldsymbol{k}| = (b^2/12) = 8.33 \cdot 10^{-10}\ m^2$. For simplicity reasons, it is also assumed that their hydraulic aperture equals the increase of the mechanical aperture and does not change with pressure.

The seeds are uniformly distributed inside a 300m × 300 m ×568m orthogonal rectangular parallelepiped that surrounds the well. Three normal distributions are employed for the values of the principal stresses and *60,000* seeds are sampled, which can have any orientation (uniform distribution). The mean values of these distributions are $\left\langle \boldsymbol{\sigma}_1^i \right\rangle = 185.0\ MPa$, $\left\langle \boldsymbol{\sigma}_2^i \right\rangle = 90.0\ MPa$ and $\left\langle \boldsymbol{\sigma}_3^i \right\rangle = 75.0\ MPa$, and their standard deviations equal *37.0 MPa*, 13.5 *MPa* and *7.5 MPa*, respectively. Cohesion C^i equals *2.0 MPa* and the friction coefficient is *0.6*. The seed model considers that the hydrostatic pressure is *45.0 MPa* everywhere. The principal stress $\boldsymbol{\sigma}_2$ is vertical, while $\boldsymbol{\sigma}_1$ and $\boldsymbol{\sigma}_3$ are parallel to vectors $(1, 1, 0)^T$ and $(-1, 1, 0)^T$, respectively. Sampled principal stresses can never be larger than *232.0 MPa* or less than *45.0 MPa* and seeds that require fluid pressure larger than *140.0 MPa* in order to be triggered are re-sampled. The b-value for each seed is $b^i = 3.5$ for $\Delta\sigma^i > 136.0\ MPa$ and $b^i = 1 - \left((1-3.5)/136\right) \cdot \Delta\sigma^i$, otherwise. All the sampled pole vectors as well as the fluid pressure value that triggers each one of them can be seen in the stereoplot in Fig. 5b.

The evolution of the simulated well pressure during the first 10 days of simulation is plotted in Fig. 5a too. At the beginning of the stimulation, the simulated wellhead pressure increases rapidly and results to induced seismicity that quickly drops the pressure at the well. In total, exactly *3,000* seeds are triggered (out of *60,000*) and *259* discrete fractures are considered by HFR-Sim. The threshold magnitude of an earthquake above which a discrete fracture is added is *1.36597* and the minimum magnitude that is sampled is *0.4*. A plot with the magnitude of these earthquakes and the moment at which they are induced is given in Fig. 5c and a histogram of the frequency of each earthquake magnitude in Fig. 5d. Finally, the propagating cloud of induced seismicity is plotted in time in Figs. 5e-5l. Although injection stops on the *4*-th day of the stimulation, seismic events continue to be triggered and increase the size of the seismic cloud. Here, the last simulated seismic event occurs approximately 10 days after the shut-down of the well.

3.2 Simulation of production phase between the stimulated well and a second well

At this point, the EGS model consists of *259* large discrete large fractures that are embedded inside a continuum with heterogeneous permeability. In order to quantify the commercial potentials of this EGS model, a simple scenario of the production phase is considered, according to which a second inclined well is considered in a distance of *200 m* from the stimulated well. The open case of the added well is at *(x,y)= (-200 m, 100 m)* at *4.632 km* depth and ends at *(x,y)=(-200,-100)* at *5.0 km* depth. The position of the new well can be compared with the induced earthquakes and the stimulated well in Fig. 6a. The permeability increase due to smaller earthquakes is neglected here.

A pressure difference of *40.0 MPa* is applied between the two wells, where water is injected from the stimulated well at a temperature of 15^oC and is produced from the non-stimulated well at a higher temperature. The applied pressure difference is less than the maximum simulated pressure at the well and is close to the target value for many EGS projects.

The first 2.5 years of operation are simulated. The simulated flow rate between the two wells is approximately *7.5 l/s*, which indicates high impedance between the two wells since this is a circulation rate of low commercial interest. The production temperature after the first day of operation is close to $168\ ^oC$ and by the end of the 2,5 years of simulation is $10\ ^oC$ less. The evolution of the temperature of the produced fluid is plotted in Fig. 6b.

4. CONCLUSION

A hybrid model has been presented, which combines modeling of flow with stochastic geomechanic considerations. The EGS simulator 'HFR-Sim' is used for modeling flow and heat transport inside EGS models. It employs an adaptive hierarchical discrete fracture representation, which allows HFR-Sim to be coupled with stochastic models that model induce seismicity. At each iteration

step, the pressure field is computed by HFR-Sim and the seed model updates the catalog of seismicity with new events. The large earthquake events introduce new discrete fractures in the EGS model and the smaller ones affect the permeability of the damaged matrix. All the considered fractures have a size and an orientation consistent with the seed model. This hybrid model will be used for near-real time probabilistic induced seismicity hazard assessments. Additionally, the EGS model obtained by the end of each simulation is employed by HFR-Sim and simulations of production phase are performed on them in order to quantitatively assess potential of generating power. Exemplary simulations have been performed with this novel hybrid model, have been presented and discussed.

ACKNOWLEDGEMENTS

The authors appreciate the support of Geo-Energie Suisse in the development of this near real time traffic light.

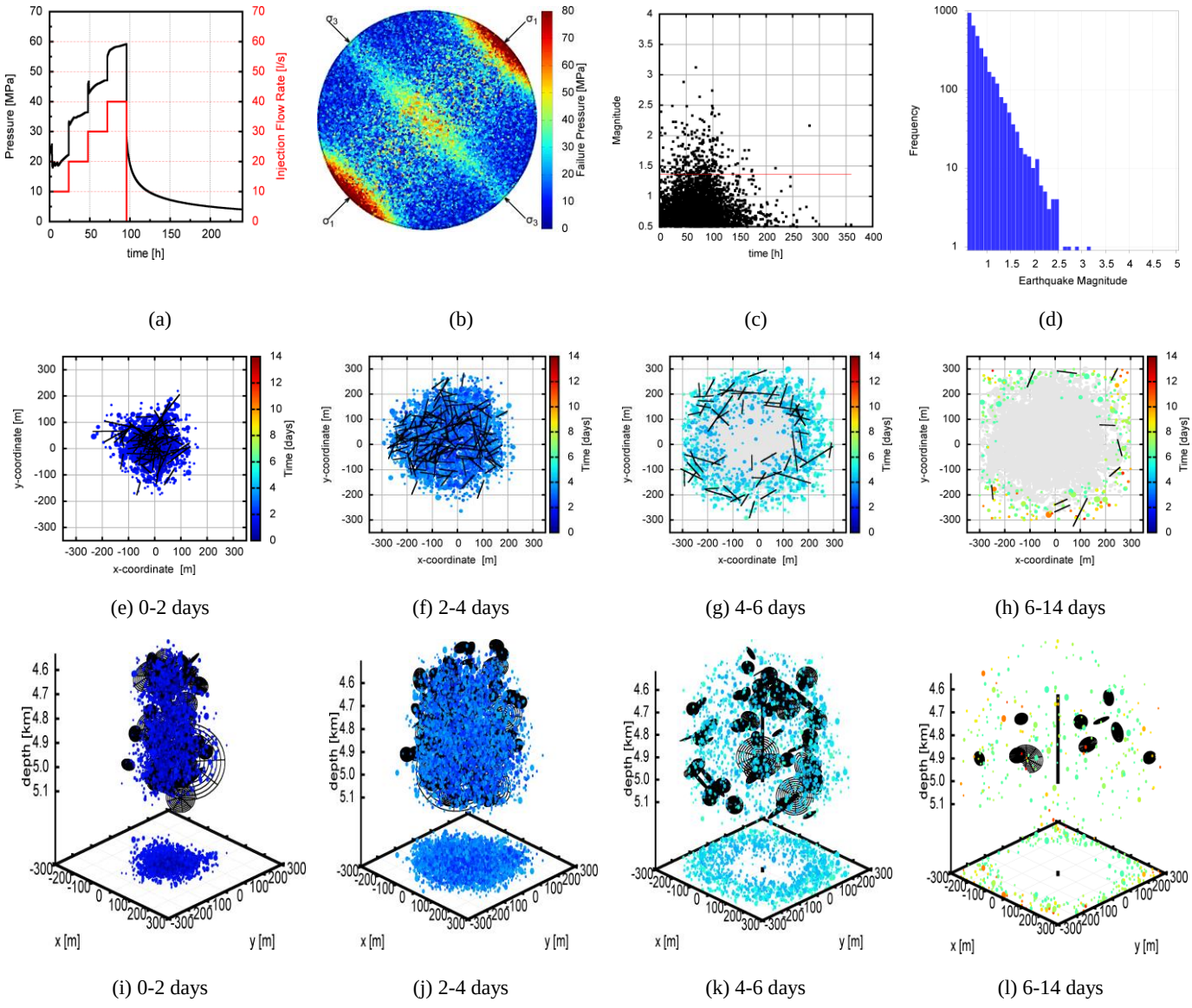

Figure 5: (a) The assumed injection strategy is shown as well as the evolution of the simulated well pressure. (b) The pole vectors of all seeds are plotted in this stereoplot and are compared with the direction of the principal compressive stresses. The color of each seed indicates the fluid pressure that is required in order to trigger this seed. It is noted, that all pole vectors have a direction towards the surface and this stereoplot shows the projection of these vectors. (c) Each dot corresponds to a seed which is triggered at that moment and produces an earthquake of that magnitude. The seeds above the thin red line introduce discrete fractures to the flow model of HFR-Sim. (d) The number of induced earthquakes with a certain magnitude is plotted in this historgram. (e)-(l) The epicenters of the induced seismicity are plotted versus time. Earthquakes with a magnitude smaller than 1.36597 are represented as colored circles with time and earthquakes with magnitude larger than that are represented with black discrete fractures. Figs. (e)-(h) are map views of the seismicity, where the strike line of the large discrete fractures is plotted. Figs. (i)-(l) are three-dimensional plots with the position in space of all small earthquakes (colored dots) and the position in space of the large HFR-Sim fractures (black discs).

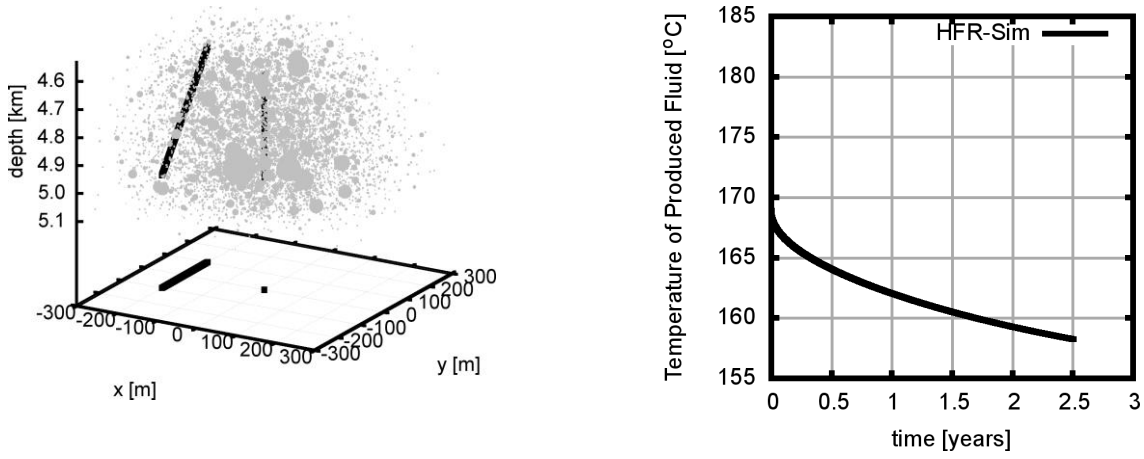

Figure 6: On the left, the position of the added inclined well is plotted with the simulated cloud of induced earthquakes. On the right, the production history is plotted for this EGS model and for an operation period of 2.5 years.

REFERENCES

Bachmann C., and Wiemer S., and Woessner J., and Hainzl S.: Statistical analysis of the induced Basel 2006 earthquake sequence: Introducing a probability-based monitoring approach for Enhanced Geothermal Systems. *Geophys. J. Int.*, **186,** (2011), 793–807.

Bertani R.: Geothermal power generation in the world 2005–2010 update report. *Geothermics*, **41**, (2012), 1–29. doi:10.1016/j.geothermics.2011.10.001

Bruel D., and Jeong W.C.: Numerical modeling of the coupling between mechanical and hydraulic properties in a granite rock mass subject to high-pressure injection experiments. (2001)

Eshelby J. D.: The Determination of the Elastic Field of an Ellipsoidal Inclusion, and Related Problems, Proceedings of the Royal Society of London. Series A, *Mathematical and Physical Sciences* , **241**, No. 1226, (1957), pp. 376-396

Gischig V. S., and Wiemer S.: A stochastic model for induced seismicity based on non-linear pressure diffusion and irreversible permeability enhancement. *Geophysical Journal International*, **194**(2), (2013) 1229–1249. doi:10.1093/gji/ggt164

Goertz-Allmann B. P., and Wiemer S.: Geomechanical modeling of induced seismicity source parameters and implications for seismic hazard assessment. *GEOPHYSICS*, **78**(1), (2013), KS25–KS39. doi:10.1190/geo2012-0102.1

Hanks T. C., and Kanamori H.: A moment magnitude scale. *Journal of Geophysical Research*, **84**(B5), (1979), 2348. doi:10.1029/JB084iB05p02348

Jung Reinhard: EGS — Goodbye or Back to the Future 95, Effective and Sustainable Hydraulic Fracturing, Dr. Rob Jeffrey (Ed.), (2013), DOI: 10.5772/56458

Karvounis, D., and Jenny P.: Modeling of Flow and Transport in Enhanced Geothermal Systems. *Proceedings*, Thirty-Sixth Workshop on Geothermal Reservoir Engineering. Stanford University, Stanford, California, USA. (2011)

Karvounis, D. C.: Simulations of enhanced geothermal systems with an adaptive hierarchical fracture representation. *PhD Dissertation*, (2013) ETH. doi:10.3929/ethz-a-009967366

Kraft T., and Mai P. M., and Wiemer S., and Deichmann N., and Ripperger J., and Kästli P., and Bachmann C., and et al.: Enhanced Geothermal Systems: Mitigating Risk in Urban Areas. *Eos, Transactions American Geophysical Union*, **90**(32), (2009), 273. doi:10.1029/2009EO320001

Kohl T., and Evans K. F., and Hopkirk R. J., and Rybach L.: Coupled hydraulic, thermal and mechanical considerations for the simulation of hot dry rock reservoirs. *Geothermics*, **24**(3), (1995) 345–359. doi:10.1016/0375-6505(95)00013-G

McClure, M.: Modeling and Characterization of Hydraulic Stimulation and Induced Seismicity in Geothermal and Shale Gas Reservoirs, *PhD Thesis*, (2012)

McClure M. W., and Horne R. N.: Investigation of injection-induced seismicity using a coupled fluid flow and rate/state friction model. *GEOPHYSICS*, **76**(6), (2011), WC181–WC198. doi:10.1190/geo2011-0064.1

Mena, B., Wiemer S., and Bachmann C. E.: Building Robust Models to Forecast the Induced Seismicity Related to Geothermal Reservoir Enhancement. *Bulletin of the Seismological Society of America*, **103**(1), (2013), 383–393. doi:10.1785/0120120102

Mourzenko, V., Thovert, J.-F., & Adler, P.: Percolation of three-dimensional fracture networks with power-law size distribution. *Physical Review E*, *72*(3), 036103, (2005). doi:10.1103/PhysRevE.72.036103

Ogata, Y.: Detection of precursory relative quiescence before great earthquakes through a statistical model, *J. geophys. Res.*, **97,** (1992), 19 845–19 871.

Peaceman, D. W. (1978). Interpretation of Well-Block Pressures in Numerical Reservoir Simulation (includes associated paper 6988). Society of Petroleum Engineers Journal, 18(3), 183–194. doi:10.2118/6893-PA

Shapiro S. A., and Dinske C., and Langenbruch C., and Wenzel F.:Seismogenic index and magnitude probability of earthquakes induced during reservoir fluid stimulations, *The LeadingEdge - Special Section: Microseismic*, (2010), 304-309

Subir K. Sanyal, and Steven J. Butler, and Daniel Swenson, and Brian Hardeman: Review of the state-of-the-art of numerical simulation of Enhanced Geothermal Systems. In *Proceedings World GeothermalCongress 2000, Kyushu - Tohoku, Japan, May 28 - June 10, 2000.*